OPEN

Hydrothermal Fabrication of Hierarchically Anatase TiO$_2$ Nanowire arrays on FTO Glass for Dye-sensitized Solar Cells

Wu-Qiang Wu, Bing-Xin Lei, Hua-Shang Rao, Yang-Fan Xu, Yu-Fen Wang, Cheng-Yong Su & Dai-Bin Kuang

MOE Key Laboratory of Bioinorganic and Synthetic Chemistry, KLGHEI of Environment and Energy Chemistry, State Key Laboratory of Optoelectronic Materials and Technologies, School of Chemistry and Chemical Engineering, Sun Yat-Sen University, Guangzhou 510275, P. R. China.

Hierarchical anatase TiO$_2$ nano-architecture arrays consisting of long TiO$_2$ nanowire trunk and numerous short TiO$_2$ nanorod branches on transparent conductive fluorine-doped tin oxide glass are successfully synthesized for the first time through a facile one-step hydrothermal route without any surfactant and template. Dye-sensitized solar cells based on the hierarchical anatase TiO$_2$ nano-architecture array photoelectrode of 18 μm in length shows a power conversion efficiency of 7.34% because of its higher specific surface area for adsorbing more dye molecules and superior light scattering capacity for boosting the light-harvesting efficiency. The present photovoltaic performance is the highest value for the reported TiO$_2$ nanowires array photoelectrode.

D ye-sensitized solar cells (DSSCs) as one of the promising alternatives to conventional silicon solar cells have attracted immense scientific and industrial research interests owing to their low cost for the material and production, excellent photoelectrical conversion efficiency[1–5]. The typical TiO$_2$ nanoparticle based photoelectrode showed significant power conversion efficiency (PCE) due to the huge surface area for the loading of dye molecules. However, the disordered stacking of TiO$_2$ nanocrystallines limits the electron transport and reduces the electron lifetime because of the random network of crystallographically misaligned crystallites, and lattice mismatches at the grain boundaries[6–9], which impedes the further improvement of the PCE. Hence, one-dimensional (1D) nanostructures such as nanorods (NRs), nanowires (NWs) or nanotubes (NTs) have been studied as photoanode materials for DSSCs and shown respectable photovoltaic performance owing to their excellent electron transport and light scattering ability[10–14]. However, almost all of the solution-phase synthesized TiO$_2$ NW arrays on fluorine doped tin oxide (FTO) glass were rutile TiO$_2$ because of very small lattice mismatch ($<$2%) between FTO and rutile TiO$_2$[15–17]. On the other hand, superior photovoltaic performance were normally obtained for anatase TiO$_2$ compared to the rutile structure resulting from larger amount of absorbed dye and faster electron transport rate[18]. Our recent report on the hierarchical anatase TiO$_2$ nanowire arrays on Ti foil has shown significant enhancement of photovoltaic performance compared to that of TiO$_2$ nanowire without the branches[11]. In addition, another indirect route via synthesizing anatase TiO$_2$ nanowires powders first and then fabricating photoanodes through screen-printing method was reported[19], but one can notice that there is still a big challenge for the direct growth of anatase TiO$_2$ NW on the FTO glass since a large lattice mismatch of $\sim$19% between FTO and anatase TiO$_2$[14]. Recently, a reactive pulsed DC magnetron sputtering method to fabricate vertically aligned anatase TiO$_2$ nanowire arrays on FTO glass was demonstrated, but its application in DSSCs was still limited by its high-technical requirements as well as difficulty in prolonging the length of nanowires[20]. Furthermore, it is generally believed that high specific surface area, fast electron transport and pronounced light-scattering capacity play salient roles in achieving high efficiency DSSC[21,22].

Up to now, 1D TiO$_2$ NW based photoelectrode has not shown significant enhancement of PCE due to low specific surface area ascribing to larger diameter and wide gaps among neighbour NWs[23,24]. A few recent examples concerning hierarchical TiO$_2$ nanowires were either for rutile TiO$_2$ on FTO glass or anatase TiO$_2$ on the Ti foil substrate[10], which were not the most ideal photoelectrode due to the rutile phase or non-transparent substrate[25–28].
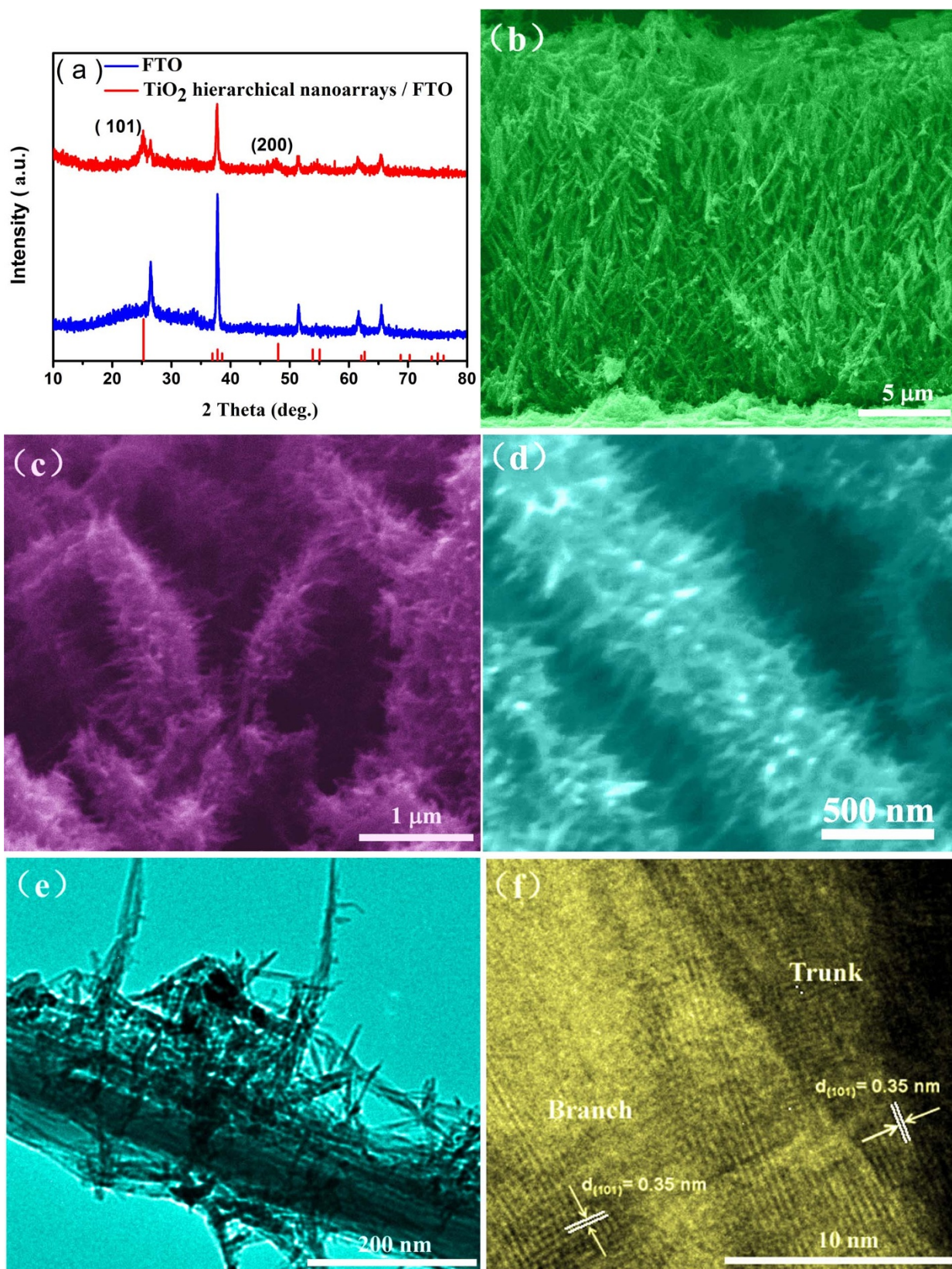
Figure 1 | X-ray diffraction patterns and electron microscopy images of as-prepared hierarchical anatase TiO₂ nano-architecture arrays prepared by a hydrothermal reaction at 180°C for 9 h on FTO glass. (a) XRD patterns of the FTO glass and the TiO₂ nanostructure/FTO glass after hydrothermal reaction, which indicate that as-prepared samples were indexed as anatase. (b, c, d) SEM images show TiO₂ nano-architecture array are hierarchical structure which is composed of long TiO₂ NW trunk covered by large amount of short NR branches. (e) TEM images reveal hierarchical TiO₂ nano-architecture arrays constituted by numerous multi-scale NRs (50–300 nm in length and approximately ~5 nm in diameter) on the surface of long TiO₂ nanowire trunk (95 nm in diameter). (f) High resolution TEM image show that both TiO₂ NW trunk and NR branch were confirmed as anatase single crystalline.

Hence, it is highly desirable but challenging to form a hierarchical 1D anatase TiO_2 nano-architecture array combining short NRs or nano-particles on the NW surface. To date, there have been no reports on the direct fabrication of vertically aligned hierarchical anatase TiO_2 NW arrays on FTO glass solely through hydrothermal process.

Here we demonstrate a facile one-step hydrothermal fabrication of hierarchical anatase TiO_2 nanowire arrays consisting of long TiO_2 NW trunks and short NR branches on FTO glass by immersing the FTO glass into the solution containing $K_2TiO(C_2O_4)_2$, diethylene glycol (DEG) and H_2O. DSSCs based on such kind of novel TiO_2 photoanode shows an outstanding power conversion efficiency of 7.34% accompanied by a short-circuit current density of 13.97 mA cm^{-2}, an open-circuit voltage of 826 mV, and a fill factor of 0.64.
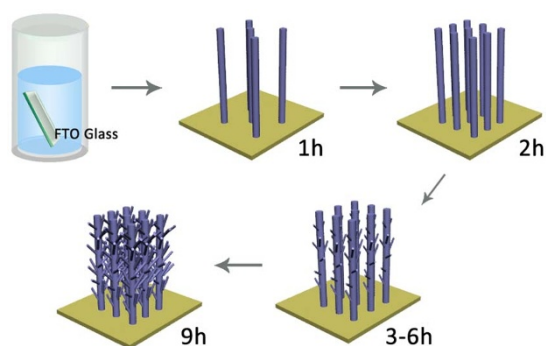
Results

Structure of hierarchically anatase TiO_2 nanowire arrays. The phase purity and structure of the hydrothermal samples were characterized by XRD measurement. The diffraction peaks of the TiO_2 nanoarrays on FTO glass (Fig. 1a) are consistent with the anatase phase (JCPDS card No.21-1272). Since no other secondary phases are observed, it's worth noting that the hierarchical anatase TiO_2 nanowire array is obtained through the present facile one-step hydrothermal reaction of $K_2TiO(C_2O_4)_2$ in water and diethylene glycol (see Method Section), which is significantly different from the previous reports on the rutile TiO_2 prepared from the hydrothermal preparation in the presence of HCl[29].

Figure 1b is a cross-sectional field emission scanning electron microscopy (FESEM image) of the synthesized TiO_2 samples/FTO glass (180°C for 9 h), showing oriented TiO_2 nanoarrays grown vertically on the FTO glass substrate with an average length of 18 μm. Higher magnification FESEM image (Fig. 1c and 1d) reveals the TiO_2 nano-architecture arrays are hierarchical structure which is composed of long TiO_2 NW trunk covered by large amount of short NR branches. Figure 1e is a typical transmission electron microscopy (TEM) image, which further illustrates the hierarchical TiO_2 nano-architecture arrays constituted by an assembly of multi-scale NRs (50–300 nm in length and approximately ~5 nm in diameter) on the surface of long TiO_2 nanowire trunk (95 nm in diameter). High resolution TEM image (Fig. 1f) taken from interfacial region of TiO_2 NW trunk and NRs branch, displays a (101) interplanar distance of 0.35 nm for both TiO_2 NW trunk and NR branch confirming the hierarchical TiO_2 nano-architecture is anatase single crystalline. Moreover, the NR branch forms the multi-angle with the long growth axis of TiO_2 NW. Some more HRTEM images of TiO_2 NW trunk and NR branches as well as typical TEM images of as-prepared

Figure 2 | Schematic formation process of hierarchically anatase TiO_2 nano-architecture arrays on FTO glass. The growth model shows the formation of hierarchically anatase TiO_2 nano-architecture arrays was intelligently assembly and the short branches became more numerous and longer on the surface of TiO_2 nanowire trunk with the prolonging reaction time.

TiO_2 nanostructure were shown in Supplementary Fig. S1 online. It is worth pointing out the single-crystal characteristics of the hierarchical 1D anatase TiO_2 nanoarrays are believed to be crucial in high efficiency DSSCs since they could be conducive to fast electron transport and reduce the possibility of surface defect trapping derived from poor crystallization[27].

Growth mechanism. To elucidate the formation of hierarchical anatase TiO_2 nano-architecture arrays on FTO glass, SEM observations of time-dependent samples during different hydrothermal reaction periods (1, 2, 3, 6, 9, 12 h) were further performed (seen in Supplementary Fig. S2 online). Moreover, Figure 2 proposes a one-step route synthesis of the novel hierarchical anatase TiO_2 nano-architecture arrays on FTO substrate. In this process, the formation of hierarchical anatase TiO_2 nano-architecture arrays was intelligently assembly without template assistance. In the initial hydrothermal stage, oriented sparse 1D TiO_2 NWs were formed on the FTO surface. Then, with the further prolongation of the hydrothermal reaction, the growth of TiO_2 NW arrays become numerous, and short NR branches start to germinate on the surface of TiO_2 NWs. Along with the increasing growth period, the branches became more numerous and longer, which could greatly enhance the filling rate in the intervals of neighbouring NWs and provide additional sites for dye adsorption. Finally, the novel hierarchical TiO_2 nano-architecture arrays consisting of long TiO_2 NW trunk and short TiO_2 NR branches on FTO glass were successfully achieved.

Photovoltaic data. It is well known that 1D nanoarrays have superior electron transport and light scattering ability compared to the nanoparticles when used as photoelectrode in dye-sensitized solar cell[30]. And the photovoltaic performance of anatase TiO_2 based DSSC is better than that of the rutile one[16]. Hence, it's of quite interesting to use the present hierarchical anatase TiO_2 nano-architecture arrays for high-efficiency DSSC since its higher surface area compared with the bare TiO_2 NW arrays ascribing from additional NR branches. Figure 3 shows the typical photocurrent density-voltage (J–V) curves and the incident photon-to-current conversion efficiency (IPCE) spectra of the solar cells based on the TiO_2 nanostructured films prepared at different hydrothermal reaction time (1, 2, 3, 6, 9, 12 h). The resultant photovoltaic parameters are summarized in Table 1. The photocurrent density (J_{sc}) increases from 3.54 to 12.50 mA cm^{-2} significantly and then slightly decreases to 12.23 mA cm^{-2} when the hydrothermal reaction time vary from 1 h to 12 h. The IPCE values (Fig. 3b) over the whole spectral range are in concurrence with the variations of J_{sc}. Among which, DSSC-9 h has the highest IPCE values (75%). The tremendous improvement of J_{sc} can be attributed to the following facts: Firstly, compared with smooth TiO_2 NWs prepared at 1 or 2 h, the increasing roughness factor for hierarchical TiO_2 nano-architecture arrays obtained at 6, 9, 12 h resulting from the additional NR branches lead to larger dye adsorption (shown in Table 1). Specifically, the amount of dye adsorption on the 9 h based hierarchical TiO_2 nano-architecture arrays is 110.0 nmol cm^{-2}, which is more than 4 times of 1 h-based TiO_2 NWs. Secondly, the TiO_2 NR branches on the main TiO_2 NW trunk fill the intervals between neighbouring NWs, which can enhance the light-scattering effects and hence improve the light-harvesting efficiency resulting in a higher J_{sc}, which was confirmed by UV-vis diffuse reflectance spectra (shown in Supplementary Fig. S3 online), and this indicates the significant improvement of light scattering capabilities for these hierarchical TiO_2 nanoarrays photoanode. Although more dye amounts and superior light scattering ability for 12 h TiO_2 based DSSC, the J_{sc} experienced a slight decrease from 12.50 (9 h based TiO_2) to 12.23 mA cm^{-2}, which can be attributed to the larger amount of surface defects and recombination centers. The photovoltage declines gradually from
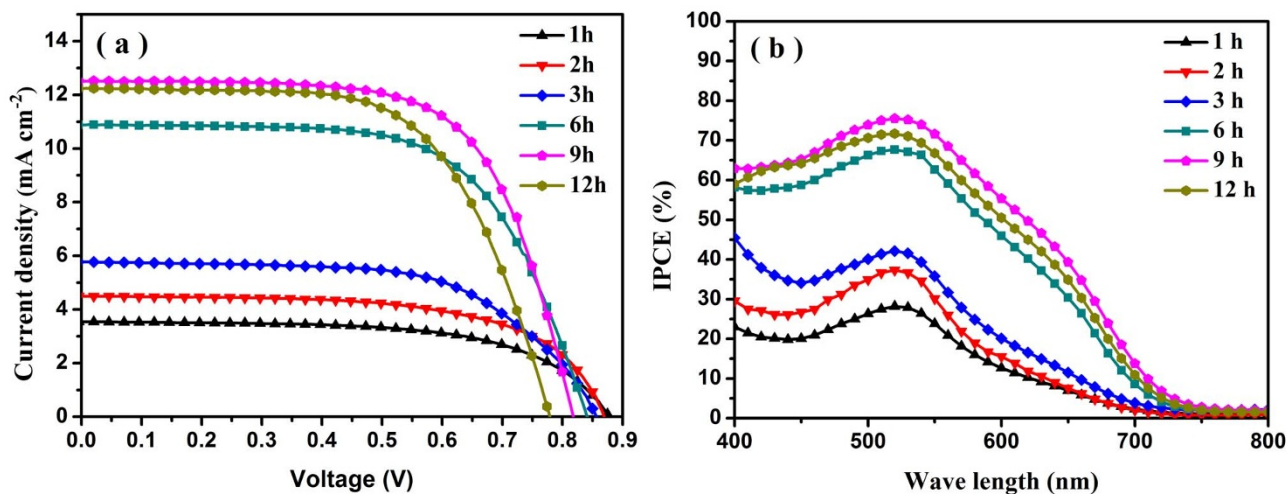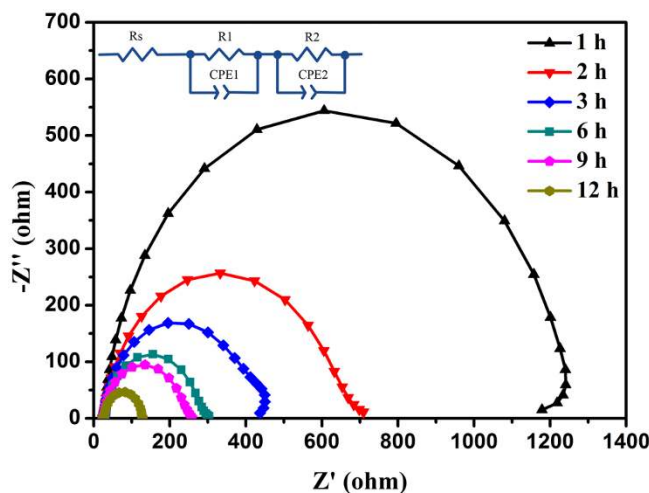
Figure 3 | **Photovoltaic characteristics using as-prepared TiO₂ nanowire array samples as photoelectrodes.** (a) J–V characteristic of DSSCs devices based on the photoelectrodes prepared at different hydrothermal reaction time measured under AM 1.5 G simulated full sunlight (100 mW cm^{-2}) illumination. (b) IPCE spectra of DSSCs based on the photoelectrodes prepared at different hydrothermal reaction time.

878 mV (DSSC-1 h) to 779 mV (DSSC-12 h) along with the increasing growth time due to the augmentation of the numerous short TiO₂ NR branches, which provides additional charge recombination sites resulting in larger recombination rate (see the following discussions of EIS, IMPS and IMVS measurement)[12]. Finally, DSSC based on 9 h based TiO₂ (DSSC-9 h) shows a PCE of 6.74%, a J_{sc} value of 12.50 mA cm^{-2}, a V_{oc} value of 818 mV and a FF value of 0.66. The outstanding photovoltaic performance for DSSC-9 h can be understood as a result of high dye loading, superior light scattering as well as considerable charge collection efficiency due to the utilization of high quality hierarchical anatase TiO₂ nano-architecture arrays.

Charge transfer dynamics. To obtain better insight into dynamics of interfacial charge transfer process within the DSSCs, electrochemical impedance spectroscopy (EIS) was performed. Figure 4 shows the Nyquist plots of the DSSCs based on above six photoelectrodes. The second semi-cycle, corresponding to the electron recombination at the TiO₂/dye/electrolyte interface, shows the recombination resistance decrease with the TiO₂ nanoarray photoelectrodes prepared at longer hydrothermal reaction time (from 1 h to 12 h) implying fast recombination reaction (or shorter electron lifetime) for the hierarchical TiO₂ nano-architecture arrays with increasing number of short TiO₂ NR branches. This may result in smaller photovoltage which is in agreement with above photovoltaic data.

Intensity-modulated photocurrent spectroscopy (IMPS) and intensity-modulated photovoltage spectroscopy (IMVS) have been further employed for the characterizations of electron transport and recombination within DSSCs, which directly relate to the J_{sc}, V_{oc} and η of DSSCs. The transport time (recombination time) can be derived from the IMPS (IMVS) measurements according to the equations:
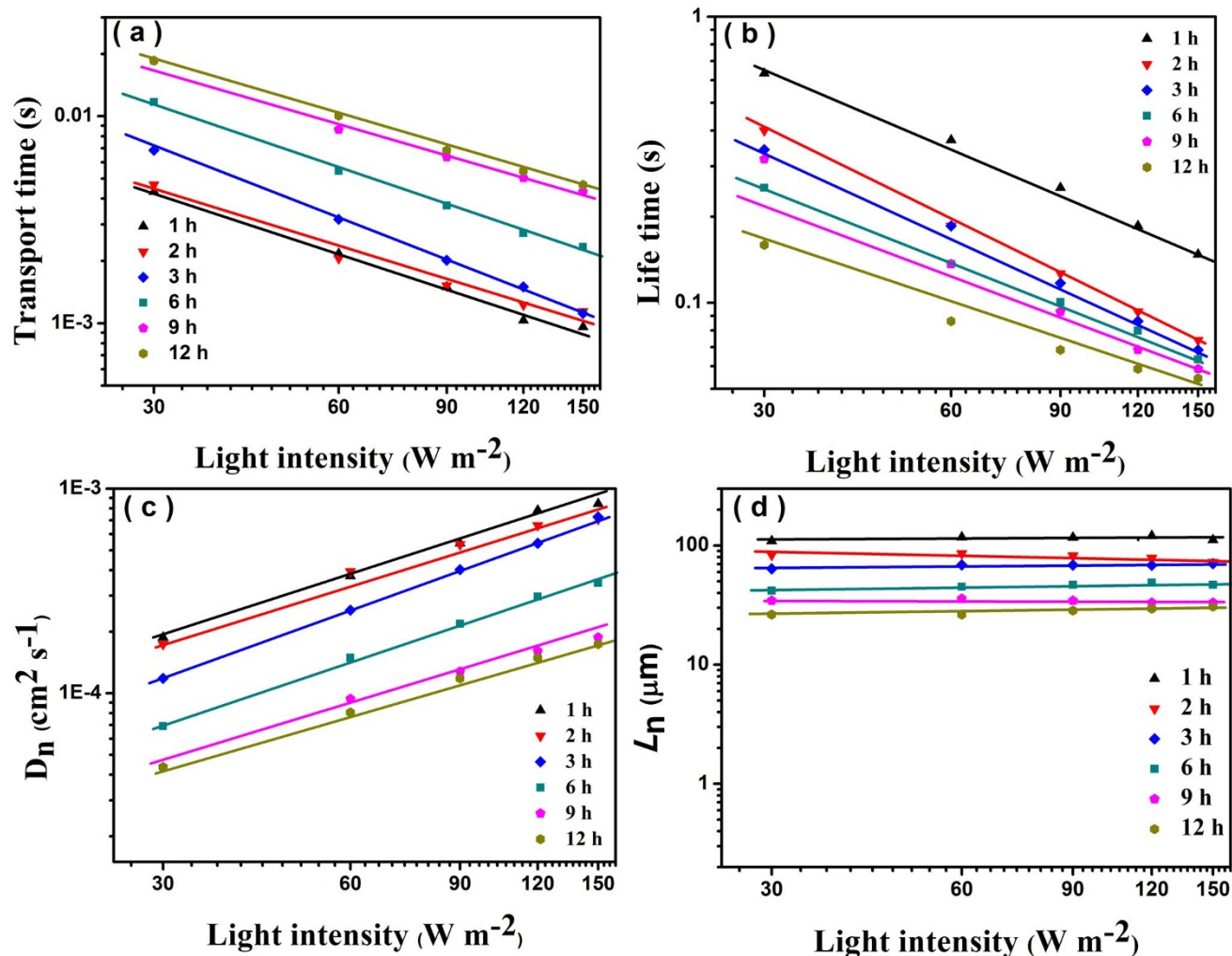
$\tau_d = 1/2\pi f_d$ ($\tau_r = 1/2\pi f_r$), where f_d (f_r) is the characteristic minimum frequency of the IMPS and IMVS imaginary component[31]. Here, τ_d and τ_r represent electron transit time across the photoanode films and recombination with I_3^- in the electrolyte, respectively. Figure 5a and 5b shows the transport and recombination times of the DSSCs based on the above six photoelectrodes as a function of light intensity. The τ_d and τ_r of the six cells decrease with the increasing light intensity. Specifically, at various light intensities, the slower transport rate (τ_d increases) and larger recombination rate (τ_r decreases) were obtained for the DSSCs based on the TiO₂ photoelectrode prepared at increasing hydrothermal time, which are attributed to more trapping sites and recombination centers for the hierarchical TiO₂ nano-architecture arrays films derived from the increasing number of TiO₂ NR branches interconnected with one another which prolong the electron transport path and hence lead to serious recombination of the DSSC. The decreasing electron lifetime (IMVS and EIS)

Table 1 | J–V characterization of the DSSCs employing 18-μm thick TiO₂ films

DSSCs	J_{sc}/mA cm^{-2}	V_{oc}/mV	η/%	FF	Adsorbed dye/nmol cm^{-2}
1 h	3.54	878	1.92	0.62	24.0
2 h	4.49	869	2.43	0.62	28.2
3 h	5.77	856	3.02	0.61	46.5
6 h	10.88	841	5.81	0.64	76.1
9 h	12.50	818	6.74	0.66	110.0
CP-9 h	13.97	826	7.34	0.64	-
12 h	12.23	779	5.96	0.63	120.0

Figure 4 | **EIS results of DSSCs based on different as-prepared samples.** Nyquist plots of the DSSCs based on different hydrothermal reaction time measured at −0.83 V bias in the dark reveal that recombination resistance decreases with the TiO₂ nanoarray photoelectrodes prepared at longer hydrothermal reaction time (from 1 h to 12 h) implying fast recombination reaction (or shorter electron lifetime) for the hierarchical TiO₂ nano-architecture arrays with increasing number of short TiO₂ NR branches.

Figure 5 | Electron transport and recombination kinetics. (a) Transport time. (b) Lifetime. (c) Electron diffusion coefficient. (d) Effective diffusion length of the DSSCs based on the photoelectrodes prepared at different hydrothermal reaction time as a function of the incident light intensity for 457 nm LED light source.

correlates with the continuing decreased V_{oc}. In addition, there is little experimental evidence concerning the comparison of light intensity dependence of the electron diffusion coefficient (D_n) and effective diffusion length between bare 1D TiO$_2$ nanowire and hierarchical TiO$_2$ nano-architecture arrays, we show here for the first time that the D_n of bare 1D TiO$_2$ NW is much more larger than that of hierarchical TiO$_2$ nano-architecture arrays at the same light intensity (Figure 5c, $D_n = d^2/(4\tau_d)$[32], d is the film thickness and τ_d is the electron transport time). The higher D_n, the faster the photo-generated electrons can transport to the anode contact. This is because the bare 1D TiO$_2$ NW photoanodes (1, 2 h) possess direct and fast electron transport pathway[28]. In contrast, hierarchical TiO$_2$ nano-architecture arrays (3, 6, 9 or 12 h) are composed of long TiO$_2$ NW trunk and numerous short TiO$_2$ NR branches would have more internal defects, in which the electron could be trapped to some extent during the process of transport. The effective electron diffusion length ($L_n = (D_n\tau_r)^{1/2}$) suggest whether the injected electron can transport to external circuit which influence the J_{sc} and η[33]. Figure 5d represents the L_n of above six DSSCs are 116.8, 82.1, 68.6, 46.9, 34.5 and 28.5 μm, respectively, which much longer than the real TiO$_2$ NW length (18 μm). This result indicates that, be it 1D TiO$_2$ nanowire or hierarchical TiO$_2$ nano-architecture arrays, the film thickness of them could be much thicker for a given recombination loss and further improving the PCE. Having considered all the

factors above, the higher short-circuit current density and power conversion efficiency of DSSC-9 h can be mainly attributed to the higher specific surface area for adsorbing more dye molecules and superior light scattering capacity for facilitating the light-harvesting efficiency compared with DSSC-1 h as well as modest electron transport rate and recombination time when compared with DSSC-12 h sample. Hence, a PCE up to 6.74% was successfully achieved for DSSC-9 h.

Effect of TiO$_2$ blocking layer on photovoltaic properties. To further improve the PCE of DSSCs, a TiO$_2$ compact layer (CP, 100 nm in thickness consisting of ~5 nm TiO$_2$ nanoparticles) was introduced between FTO glass substrate and hierarchical anatase TiO$_2$ nano-architecture arrays film by spin-coating ahead of the hydrothermal process. Figure 6b shows the photocurrent density-voltage (J–V) curves and the inset image is the IPCE spectrum of the complete hierarchical TiO$_2$ nanoarrays photoanode based DSSC (Fig. 6a). It is notable that the J_{sc}, V_{oc} and η of DSSC-CP-9 h is 13.97 mA cm^{-2}, 826 mV and 7.34%, respectively, which are much superior to that of 12.50 mA cm^{-2}, 818 mV and 6.74% for the DSSC-9 h (without TiO$_2$ compact layer). The considerable improvement of J_{sc}, V_{oc} and η by the introduction of compact TiO$_2$ blocking layer is believed to effectively reduce the charge recombination in FTO/electrolyte interface and enhance the adhesion between hierarchical
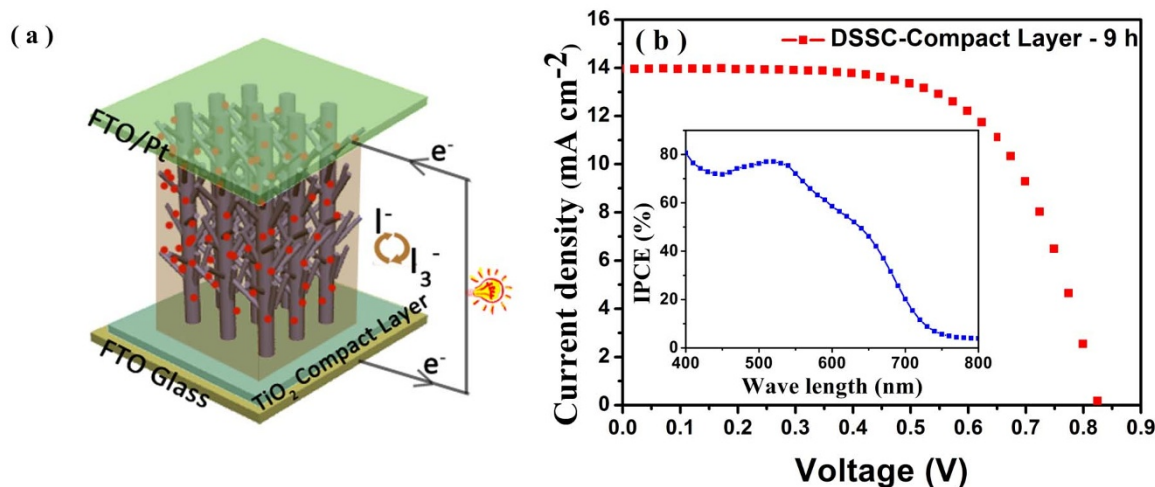
Figure 6 | Schematic diagram and photovoltaic characteristics of DSSC based on hierarchical anatase TiO₂ nanoarrays photoanode. (a) Sandwich type model of DSSC based on hierarchical anatase TiO₂ nanoarrays photoanode and platinum counter electrode. (b) J–V characterization of DSSC employing hierarchical TiO₂ nanoarrays prepared at 9 h with an additional TiO₂ blocking layer and the inset image is the corresponding IPCE spectrum.

anatase TiO₂ nano-architecture arrays and FTO glass surface due to the highly density and large contact area of quantum-size TiO₂ nanoparticles[34,35]. Consequently, electron transport would become faster and thus boost the charge transfer efficiency, leading to a 9% enhancement of power conversion efficiency.

Finally, in order to highlight the advantage of hierarchical TiO₂ nanowire arrays compared to that of P25 nanoparticle, two photo-anodes with similar dye uptakes between the P25 nanoparticle (112.2 nmol cm^{-2}, 12 μm in thickness) and hierarchical TiO₂ nanowire arrays (110.0 nmol cm^{-2}, 18 μm in thickness) were used to prepare the DSSCs. The J_{sc} and V_{oc} of P25 based DSSC are 12.01 and 794 mV, respectively, which are much lower than those of hierarchically TiO₂ nanowire arrays (13.97 mA cm^{-2} and 826 mV), leading to a significant enhancement of efficiency for the latter (7.34%) compared with the former (6.35%). The enhanced PCE can be attributed to the superior light scattering ability for increasing light-harvesting efficiency, direct electron transit pathway for fast electron transport, longer electron lifetime due to its 1D nanostructure with less grain boundaries and defects for slow charge recombination.

Discussion

A novel hierarchical anatase TiO₂ nano-architecture array consisting of long TiO₂ nanowire trunk and numerous short nanorod branches (18 μm in thickness) on transparent conductive FTO glass substrate has been successfully prepared for the first time via a simple one-step hydrothermal route without any surfactant and template. The DSSC based on such hierarchical anatase TiO₂ nano-architecture array photoelectrode showed an impressive power conversion efficiency of 7.34%, which is the highest value reported for the TiO₂ nanowire array. The investigations of EIS, IMPS and IMVS reveal that the electron transport and recombination for hierarchical anatase TiO₂ nano-architecture array are inferior to those bare TiO₂ nanowires due to the additional trapping sites and recombination centres for the former. However, the significant improvement of photocurrent for the hierarchical anatase TiO₂ nano-architecture array can be ascribed to its higher specific surface area for adsorbing more dye molecules and superior light scattering capacity for boosting the light-harvesting efficiency which are responsible for the improvement of the power conversion efficiency. We anticipate that the present mild synthesis of hierarchical anatase TiO₂ nanoarray opens up a promising avenue for scalable fabricating

high-efficiency solid-state DSSCs or quantum-dot sensitized solar cells.

Methods

Materials synthesis. 0.002 mol K₂TiO(C₂O₄)₂ was added to the mixture solvent containing 30 mL diethylene glycol (DEG) and 10 mL deionized water. After stirring of 30 min, the mixture solution was transferred to a 50 mL Teflon-lined stainless steel autoclave. Then cleaned FTO glass (ultrasonically for 10 min in acetone, 2-propanol and deionized water, respectively) or TiO₂-coated FTO glass (a 100 nm thick TiO₂ compact layer on FTO glass obtained by spin-coating of the synthesized TiO₂ colloid solution[36] followed by 30 min at 500°C in ambient air) were placed at an angle against the wall of the Teflon-liner with the conducting side facing down. The hydrothermal synthesis was conducted at 180°C for 1–12 h. After reaction, the autoclave was cooled to room temperature naturally and then the FTO glass was taken out and rinsed with deionized water, ethanol and then dried at room temperature.

Dye-sensitized solar cells fabrication. The as-prepared hierarchical anatase TiO₂ nanoarrays on FTO glass were used as photoelectrode for dye-sensitized solar cells. Prior to dye sensitization, the as-prepared TiO₂ nanoarrays were immersed into a 40 mM TiCl₄ aqueous solution at 70°C for 30 min and washed with water and ethanol, then sintered at 520°C for 30 min. After cooling down to 80°C, the TiO₂ electrodes were putted into 0.5 mM N719 dye (Ru[LL'-(NCS)₂], L = 2,2'-bipyridyl-4,4'-dicarboxylic acid, L = 2, 2'-bipyridyl-4, 4'-ditetrabutylammonium carboxylate, Solaronix Co.) in acetonitrile/tert-butanol (1 : 1 v/v), and kept for 20 h at room temperature. The Pt-coated FTO as a counter electrode was prepared by dropping H₂PtCl₆ (5 mM) solution on the FTO glass followed by heating at 400°C for 15 min in air. The electrolyte consisted of 1-propyl-3-methyl-imidazolium iodide (PMII, 0.6 M), I₂ (0.03 M), LiI (0.05 M), Guanidine thiocyanate (GuNCS, 0.1 M, Aldrich), and 4-tert-butylpyridine (t-BP, 0.5 M, Aldrich) in acetonitrile and valeronitrile (85 : 15 v/v). The active area of the dye-coated TiO₂ film was 0.16 cm².

Characterization. The phase purity of the products was characterized by X-ray diffraction (XRD) on a Bruker D8 Advance X-ray diffractometer using Cu Kα radiation (λ = 1.5418 Å). The Field emission scanning electron microscopy (FE-SEM, JSM-6330F), transmission electron microscope (TEM) and high-resolution transmission electron microscope (HRTEM) were performed on a JEOL-2010 HR transmission electron microscope to characterize the morphology, size and the intrinsic structure. The diffuse reflectance spectra and absorption spectra of desorbed-dye solution from the hierarchical TiO₂ nanowire arrays films (dye-absorbed TiO₂ film was immersed into 0.1 M NaOH aqueous solution) were measured on a UV/Vis-NIR spectrophotometer (UV-3150) to evaluate the reflectance performance and the adsorbed dye amount of TiO₂ films. The current-voltage characteristics were performed using a Keithley 2400 source meter under simulated AM 1.5 G illumination (100 mW cm^{-2}) provided by a solar light simulator (Oriel, Model: 91192). The incident light intensity was calibrated with an NREL-calibrated Si solar cell. The electrochemical impedance spectroscopy (EIS) measurements were performed with a Zennium electrochemical workstation (ZAHNER) with the frequency range from 10 mHz to 1 MHz. The magnitude of the alternative signal was 10 mV. The impedance measurements were carried out under forward bias of −0.83 V in the dark condition. Intensity-modulated photovoltage spectroscopy (IMVS) and intensity-modulated photocurrent spectroscopy (IMPS) measurements were carried out on a electrochemical workstation (Zahner, Zennium)

with a frequency response analyzer under a modulated green light emitting diodes (457 nm) driven by a source supply (Zahner, PP211), which can provide both dc and ac components of the illumination. The modulated light intensity was 10% or less than the base light intensity. The frequency range was set from 100 KHz to 0.1 Hz.

1. O'Regan, B. & Grätzel, M. A low-cost, high-efficiency solar cell based on dye-sensitized colloidal TiO_2 films. *Nature* **353**, 737–740 (1991).
2. Yella, A. *et al.* Porphyrin-Sensitized Solar Cells with Cobalt (II/III)-Based Redox Electrolyte Exceed 12 Percent Efficiency. *Science* **334**, 629–634 (2011).
3. Xin, X., He, M., Han, W., Jung, J. & Lin, Z. Low-cost copper zinc tin sulfide counter electrodes for high-efficiency dye-sensitized solar cells. *Angew. Chem. Int. Ed.* **50**, 11739–11742 (2011).
4. Yum, J.-H. *et al.* A cobalt complex redox shuttle for dye-sensitized solar cells with high open-circuit potentials. *Nat Commun* **3**, 631 doi:10.1038/ncomms1655 (2012).
5. Kim, H.-S. *et al.* Lead iodide perovskite sensitized all-solid-state submicron thin film mesoscopic solar cell with efficiency exceeding 9%. *Sci. Rep.* **2:591**, 1–7 (2012).
6. Bierman, M. J. & Jin, S. Potential applications of hierarchical branching nanowires in solar energy conversion. *Energ Environ. Sci.* **2**, 1050–1059 (2009).
7. Hu, L. H. *et al.* Microstructure design of nanoporous TiO_2 photoelectrodes for dye-sensitized solar cell modules. *J. Phys. Chem. B* **111**, 358–362 (2007).
8. Berger, T., Lana-Villarreal, T., Monllor-Satoca, D. & Gomez, R. An electrochemical study on the nature of trap states in nanocrystalline rutile thin films. *J. Phys. Chem. C* **111**, 9936–9942 (2007).
9. Qu, J., Li, G. R. & Gao, X. P. One-dimensional hierarchical titania for fast reaction kinetics of photoanode materials of dye-sensitized solar cells. *Energy Environ. Sci.* **3**, 2003–2009 (2010).
10. Liao, J. Y., Lei, B. X., Chen, H. Y., Kuang, D. B. & Su, C. Y. Oriented hierarchical single crystalline anatase TiO_2 nanowire arrays on Ti-foil substrate for efficient flexible dye-sensitized solar cells. *Energy Environ. Sci.* **5**, 5750–5757 (2012).
11. Liao, J. Y., Lei, B. X., Kuang, D. B. & Su, C. Y. Tri-functional hierarchical TiO_2 spheres consisting of anatase nanorods and nanoparticles for high efficiency dye-sensitized solar cells. *Energ Environ. Sci.* **4**, 4079–4085 (2011).
12. Ohsaki, Y. *et al.* Dye-sensitized TiO_2 nanotube solar cells: fabrication and electronic characterization. *Phys. Chem. Chem. Phys.* **7**, 4157–4163 (2005).
13. Zhu, K., Neale, N. R., Miedaner, A. & Frank, A. J. Enhanced charge-collection efficiencies and light scattering in dye-sensitized solar cells using oriented TiO_2 nanotubes arrays. *Nano Letters* **7**, 69–74 (2007).
14. Feng, X., Shankar, K., Paulose, M. & Grimes, C. A. Tantalum-doped titanium dioxide nanowire arrays for dye-sensitized solar cells with high open-circuit voltage. *Angew. Chem. Int. Ed.* **48**, 8095–8098 (2009).
15. Howard, C., Sabine, T. & Dickson, F. Structural and thermal parameters for rutile and anatase. *Acta Crystallogr. Sect. B* **47**, 462–468 (1991).
16. Sedach, P. A. *et al.* Solution growth of anatase TiO_2 nanowires from transparent conducting glass substrates. *J. Mater. Chem.* **20**, 5063–5069 (2010).
17. Wang, X. Y. *et al.* Synthesis of long TiO_2 nanowire arrays with high surface areas via synergistic assembly route for highly efficient dye-sensitized solar cells. *J. Mater. Chem.* **22**, 17531–17538 (2012).
18. Park, N. G., van de Lagemaat, J. & Frank, A. J. Comparison of Dye-Sensitized Rutile- and Anatase-Based TiO_2 Solar Cells. *J. Phys. Chem. B* **104**, 8989–8994 (2000).
19. Yu, X. *et al.* One-step ammonia hydrothermal synthesis of single crystal anatase TiO_2 nanowires for highly efficient dye-sensitized solar cells. *J. Mater. Chem. A* **1**, 2110–2117 (2013).
20. In Su, II. *et al.* Low temperature synthesis of transparent, vertically aligned anatase TiO_2 nanowire arrays: application to dye sensitized solar cells. *Bull. Korean Chem. Soc.* **33**, 1989–1992 (2012).
21. Zhang, Q., Chou, T. P., Russo, B., Jenekhe, S. A. & Cao, G. Aggregation of ZnO nanocrystallites for high conversion efficiency in dye-sensitized solar cells. *Angew. Chem. Int. Ed.* **47**, 2402–2406 (2008).
22. Qiu, Y. C., Chen, W. & Yang, S. H. Double-Layered Photoanodes from Variable-Size Anatase TiO_2 Nanospindles: A Candidate for High-Efficiency Dye-Sensitized Solar Cells. *Angew. Chem. Int. Ed.* **49**, 3675–3679 (2010).
23. Roy, P., Kim, D., Parasivam, I. & Schmuki, P. Improved efficiency of TiO_2 nanotubes in dye sensitized solar cells by decoration with TiO_2 nanoparticles. *Electrochem. Commun.* **11**, 1001–1004 (2009).
24. Wu, W.-Q. *et al.* Dye-sensitized solar cells based on a double layered TiO_2 photoanode consisting of hierarchical nanowire arrays and nanoparticles with greatly improved photovoltaic performance. *J. Mater. Chem.* **22**, 18057–18062 (2012).
25. Zhuge, F. W. *et al.* Toward Hierarchical TiO_2 Nanotube Arrays for Efficient Dye-Sensitized Solar Cells. *Adv. Mater.* **23**, 1330–1334 (2011).
26. Wang, H. *et al.* Rutile TiO_2 nano-branched arrays on FTO for dye-sensitized solar cells. *Phys. Chem. Chem. Phys.* **13**, 6977–6982 (2011).
27. Feng, X. J. *et al.* Vertically Aligned Single Crystal TiO_2 Nanowire Arrays Grown Directly on Transparent Conducting Oxide Coated Glass: Synthesis Details and Applications. *Nano Letters* **8**, 3781–3786 (2008).
28. Lv, M. *et al.* Densely aligned rutile TiO_2 nanorod arrays with high surface area for efficient dye-sensitized solar cells. *Nanoscale* **4**, 5872–5879 (2012).
29. Liu, B. & Aydil, E. S. Growth of Oriented Single-Crystalline Rutile TiO_2 Nanorods on Transparent Conducting Substrates for Dye-Sensitized Solar Cells. *J. Am. Chem. Soc.* **131**, 3985–3990 (2009).
30. Feng, X., Zhu, K., Frank, A. J., Grimes, C. A. & Mallouk, T. E. Rapid charge transport in dye-sensitized solar cells made from vertically aligned single-crystal rutile TiO_2 nanowires. *Angew. Chem. Int. Ed.* **51**, 2727–2730 (2012).
31. Wang, H. X., Nicholson, P. G., Peter, L., Zakeeruddin, S. M. & Gratzel, M. Transport and Interfacial Transfer of Electrons in Dye-Sensitized Solar Cells Utilizing a Co(dbbip)$_2$ Redox Shuttle. *J. Phys. Chem. C* **114**, 14300–14306 (2010).
32. Dloczik, L. *et al.* Dynamic response of dye-sensitized nanocrystalline solar cells: Characterization by intensity-modulated photocurrent spectroscopy. *J. Phys. Chem. B* **101**, 10281–10289 (1997).
33. Jennings, J. R., Ghicov, A., Peter, L. M., Schmuki, P. & Walker, A. B. Dye-sensitized solar cells based on oriented TiO_2 nanotube arrays: Transport, trapping, and transfer of electrons. *J. Am. Chem. Soc.* **130**, 13364–13372 (2008).
34. Ito, S. *et al.* Control of dark current in photoelectrochemical ($TiO_2/I^{(-)} - I_3^{(-)}$) and dye-sensitized solar cells. *Chem. Commun.* 4351–4353 (2005).
35. Zhu, K., Schiff, E. A., Park, N. G., van de Lagemaat, J. & Frank, A. J. Determining the locus for photocarrier recombination in dye-sensitized solar cells. *Appl. Phys. Lett.* **80**, 685–687 (2002).
36. Scolan, E. & Sanchez, C. Synthesis and Characterization of Surface-Protected Nanocrystalline Titania Particles. *Chem. Mater.* **10**, 3217–3223 (1998).

Author contributions

W.Q.W., B.X.L. and D.B.K. proposed and designed the experiments. W.Q.W. and B.X.L. carried out the synthetic experiments. H.S.R., Y.F.W. and Y.F.X. performed the HRTEM, SEM characterization and structural analysis. D.B.K. analysed the data. W.Q.W. designed and carried out the experiments, analysed the data. W.Q.W., D.B.K. and C.Y.S. wrote the manuscript. All the authors participated in discussions of the research.

Additional information

Supplementary information accompanies this paper at http://www.nature.com/scientificreports

Competing financial interests: The authors declare no competing financial interests.

How to cite this article: Wu, W.Q. *et al.* Hydrothermal Fabrication of Hierarchically Anatase TiO_2 Nanowire arrays on FTO Glass for Dye-sensitized Solar Cells. *Sci. Rep.* **3**, 1352; DOI:10.1038/srep01352 (2013).